IEEE Photonics Journal
An IEEE Photonics Society Publication

Open Access

Optimized Single-Shot Photonic Time-Stretch Digitizer Using Complementary Parallel Single-Sideband Modulation Architecture and Digital Signal Processing

Volume 9, Number 3, June 2017

Di Peng
Zhiyao Zhang
Yangxue Ma
Yali Zhang
Shangjian Zhang, *Member, IEEE*
Yong Liu, *Senior Member, IEEE*

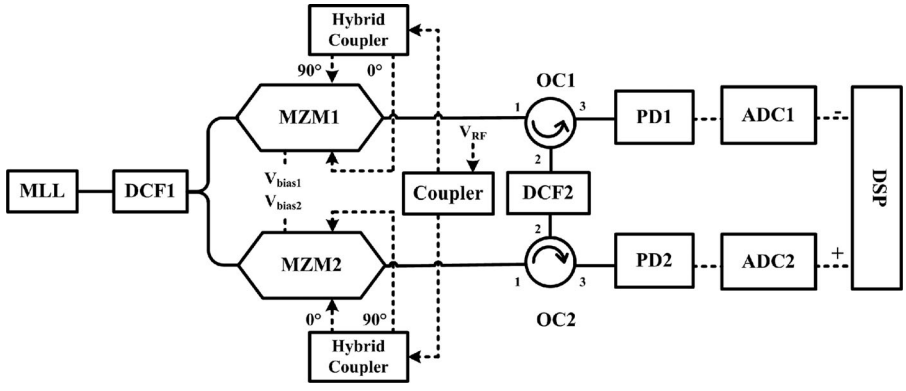

DOI: 10.1109/JPHOT.2017.2694442
1943-0655 © 2017 IEEE

IEEE photonics SOCIETY

IEEE

Optimized Single-Shot Photonic Time-Stretch Digitizer Using Complementary Parallel Single-Sideband Modulation Architecture and Digital Signal Processing

Di Peng,[1,2] Zhiyao Zhang,[1,2] Yangxue Ma,[1,2] Yali Zhang,[1,2] Shangjian Zhang,[1,2] *Member, IEEE*, and Yong Liu,[1,2] *Senior Member, IEEE*

[1]State Key Laboratory of Electronic Thin Films and Integrated Devices, School of Optoelectronic Information, University of Electronic Science and Technology of China, Chengdu 610054, China
[2]Collaboration Innovation Center of Electronic Materials and Devices, University of Electronic Science and Technology of China, Chengdu 610054, China

DOI:10.1109/JPHOT.2017.2694442

Manuscript received February 20, 2017; revised April 1, 2017; accepted April 11, 2017. Date of publication April 17, 2017; date of current version May 3, 2017. This work was supported in part by the National Nature Science Foundation of China under Grant 61421002, Grant 61575037, and Grant 61307031; in part by the Innovation Funds of Collaboration Innovation Center of Electronic Materials and Devices (No. ICEM2015-2001); and in part by the China Scholarship Council under Grant 201606075076.
Corresponding author: Zhiyao Zhang (e-mail: zhangzhiyao@uestc.edu.cn).

Abstract: A novel single-shot photonic time-stretch digitizer scheme is proposed based on complementary parallel single-sideband modulation architecture. Successive digital signal processing, including linearization operation and phase compensation, is employed to improve the performance. Both theoretical analysis and simulation results show that the proposed scheme can simultaneously solve the three vital problems in the single-shot photonic time-stretch digitizers, i.e., removal of the dynamic pulse envelope variation, the dispersion-induced penalty, and suppression of the modulation-induced distortion. Hence, the proposed single-shot photonic time-stretch digitizer can overcome the dispersion-induced bandwidth limitation and realize linearization performance.

Index Terms: Analog-to-digital conversion, microwave photonics, nonlinear distortion, single-sideband modulation, time stretch.

1. Introduction

The ability to digitize an ultra-wideband signal in real time is urgently required in various applications such as capturing ultrafast non-repetitive transients and recording data streams with a bit rate up to multi-hundred Gb/s [1], [2]. Due to the limited speed of sample-and-hold circuit, it is difficult for real-time oscilloscopes to have an input bandwidth beyond multi-tens of GHz [3]. In addition, the sampling rate is constrained to be less than multi-hundreds of GS/s on account of the restricted effective number of bits (ENOB) due to sampling time jitter, comparator ambiguity and channel mismatch if interleaving scheme is employed [4] (e.g., advanced real-time oscilloscope of Tektronix DPO77002SX is merely with an input bandwidth of 70 GHz and a sampling rate of 200 GS/s).

One potential approach to break the electronic bottleneck is employing photonic time-stretch technology to slow down the input signal before its digitization [5], [6]. Through time-stretch preprocessing, the sampling rate and the input bandwidth of digitizers can be enhanced by a multiple of time-stretch ratio in principle [7], [8]. To date, real-time digitization at 10 TS/s has already been demonstrated using a real-time oscilloscope with a sampling rate of 40 GS/s [9]. However, the time aperture in [9] is not sufficient for recording a signal with duration exceeding 600 ps. The favorable way to enlarge the time aperture while maintaining the time-stretch ratio is increasing the optical bandwidth like using a supercontinuum source [10]. Nevertheless, the low power spectrum density in a supercontinuum source may deteriorate the signal-to-noise ratio (SNR) of the time stretch system. Therefore, in practical systems, passive mode-locked optical sources with relatively condensed spectra are generally employed. For these systems, the only way to enhance the time aperture is increasing the group-velocity dispersion, which, however, may lead to the dispersion-induced power penalty problem.

The dispersion-induced power penalty puts a stringent limit to the bandwidth enhancement especially when large group-velocity dispersion is adopted in the time-stretch preprocessor for realizing both a great time window and a large time-stretch factor. Moreover, it may also reduce the SNR if the input signal frequency is in the vicinity of the transmission notch. So far, there are two effective methods that have been proposed to settle this trouble. The first one is employing single-sideband (SSB) modulation which converts the dispersion-induced frequency-related power penalty into the dispersion-induced frequency-related phase shift, thus eliminating the power-fading-related bandwidth limit and the SNR degradation [11], [12]. The alternative one is adopting phase diversity technology where the 90-degree phase difference between the two output ports of a dual-output single-arm-drive Mach-Zehnder electro-optic modulator can be utilized to mitigate the frequency fading problem based on the maximum ratio combining algorithm [13].

In addition, the vertical accuracy (evaluated by ENOB) is another focus issue in a photonic time-stretch digitizer, which is stringently related to the signal-to-noise and distortion ratio (SINAD) and generally limited by the signal distortion in the time stretch process. There are many physical mechanisms that lead to signal distortion such as dynamic carrier envelope variation, modulation nonlinearity, limited optical bandwidth, higher order dispersion, and nonlinear optical effect [14]. Among these constraints, the dynamic carrier envelope variation and the modulation nonlinearity are the dominate contributor, and should be definitely suppressed to enhance the ENOB of the photonic time-stretch digitizer. The former one originates from the fact that the chirped pulse used as optical carrier is generally not flat and varies from pulse to pulse, which introduces a severe distortion to the stretched signal. Fortunately, this issue can be effectively solved through using a dual-output push-pull Mach-Zehnder electro-optic modulator whose outputs are complementary without extra phase modulation [15]. The latter problem is attributed to that the transmission response of a Mach-Zehnder electro-optic modulator is intrinsically a nonlinear one, which brings distortion products limiting the spur-free dynamic range (SFDR). Various solutions have been proposed to settle this puzzle. For example, optimization of bias points or structural parameters in diverse modulator structures can be used to efficiently suppress the even-order distortions or the third-order spurs [16], [17]. Besides, post-compensation in the digital domain is capable of canceling the even-order harmonics and suppressing the third-order intermodulation distortions [17]–[20].

A single-shot photonic time-stretch digitizer is attractive for practical applications only if it is simultaneously with a great time window, a large time-stretch factor, an ultra-wide bandwidth and a high SINAD [6], [14]. Although these targets can be achieved independently based on the above-mentioned technologies, an overall scheme which has the ability to simultaneously improve all of the above-mentioned constraints using a single modulation scheme is still absent, to the best of authors' knowledge.

In this paper, a novel scheme of single-shot photonic time-stretch digitizer is proposed to simultaneously remove the pulse-envelope-induced distortion, the dispersion-induced power penalty, and suppress the modulation distortion products. The proposed scheme is based on parallel SSB modulation architecture with each modulator biased at the quadrature point of the rising and falling

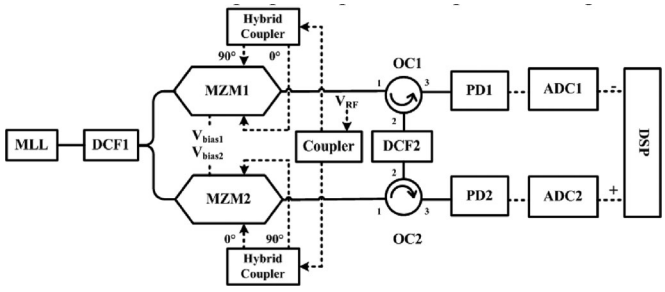

Fig. 1. Architecture of the proposed single-shot photonic time-stretch digitizer. MLL: mode-locked laser, DCF: dispersion compensation fiber, MZM: Mach-Zehnder modulator, OC: optical circulator, PD: photodetector, ADC: analog-to-digital converter, DSP: digital signal processing. Solid line: optical path; dashed line: electrical path.

edges of the transmission curve, respectively. In the proposed scheme, SSB modulation and phase compensation algorithm can help to reduce the power penalty and enhance the time-bandwidth product. The dynamic pulse envelope variation and the modulation-induced distortion can be suppressed through linearization operation in the digital domain. Most important of all, the proposed scheme can be realized using the devices off the shelf. Both theoretical analysis and numerical simulation show that the proposed scheme is available for realizing a single-shot photonic time-stretch digitizer with dispersion penalty-free and linearization performance.

2. Operation Principle

Fig. 1 shows the architecture of the proposed single-shot photonic time-stretch digitizer. Firstly, the ultra-short optical pulses generated by a passive mode-locked laser (MLL) perform time-wavelength mapping and transform into linearly chirped ones after passing through the first spool of dispersion compensation fiber (DCF1). Then, two dual-drive Mach-Zehnder modulators (MZMs) in parallel, each with a radio-frequency (RF) hybrid coupler, are employed to modulate the input RF signal onto the envelope of the two chirped pulse duplicates via SSB modulation. Specifically, the two MZMs are biased at the quadrature point of the falling and rising edges of the transmission curve, respectively, which is critically important to remove the pulse-envelope-induced distortion and suppress the modulation-induced harmonic distortion. Subsequently, the two modulated pulses enter and counter-propagate with each other in the second spool of dispersion compensation fiber (DCF2) through two optical circulators (OC1 and OC2), experiencing identical time stretch. After that, two slowed-down RF signals are demodulated from the corresponding optical pulse envelope by photodetectors (PDs), and digitalized by an analog-to-digital converter (ADC) successively. Finally, the two digitized data stream are sent to the digital signal processing (DSP) module to remove the dynamic pulse envelope variation and the dispersion-induced phase penalty, as well as to suppress the modulation-induced nonlinearity, ultimately realizing a single-shot photonic time-stretch digitizer with broadband and linearization performance.

The characteristic of the proposed scheme can be summarized as follows. The SSB modulation scheme in combination with the proposed phase compensation algorithm guarantees a high SNR over a broadband frequency domain. The parallel complementary modulation architecture with the assistance of differential operation improves the system linearity. Additionally, the arcsine operation is also employed in the signal processing since it is theoretically effective to suppress the odd-order spurs in the dispersion-free application. Although its suppression effect does not always work in a dispersion system for various frequencies, it is indeed efficient for some frequencies, and the linearization performance will not be dramatically deteriorated even in the worst case. The detailed signal processing steps are presented in what follows.

Assuming the ultra-short optical pulse generated by MLL is a transform-limited Gaussian one whose optical field in the frequency domain can be given by

$$E_1(\omega) = E_0\sqrt{2\pi T_0^2}\exp\left(-\frac{T_0^2\omega^2}{2}\right) \tag{1}$$

where E_0 is the amplitude of the optical field, and T_0 is the half-width of the pulse at $1/e$ intensity. After propagating through DCF1, the field in the frequency domain can be calculated as

$$E_2(\omega) = E_1(\omega)\exp\left(\frac{j}{2}\beta_2 L_1\omega^2\right) \tag{2}$$

where β_2 and L_1 are the group-velocity dispersion (GVD) coefficient and the length of DCF1, respectively. In order to analyze the intermodulation effect, a two-tone RF signal of $V(T) = V_0/2[\cos(\omega_1 T) + \cos(\omega_2 T)]$ is used to drive the two MZMs in parallel. Thus, the time-domain optical fields at the output of the two MZMs biased at the quadrature point of falling and rising edges of the transmission curve respectively become

$$E_{3-}(T) = \frac{\sqrt{2}}{4}E_2(T)\cdot\begin{Bmatrix} -\sin\left[\frac{m}{4}\cos(\omega_1 T) + \frac{m}{4}\cos(\omega_2 T)\right] \\ +j\cos\left[\frac{m}{4}\cos(\omega_1 T) + \frac{m}{4}\cos(\omega_2 T)\right] \\ +\cos\left[\frac{m}{4}\sin(\omega_1 T) + \frac{m}{4}\sin(\omega_2 T)\right] \\ +j\sin\left[\frac{m}{4}\sin(\omega_1 T) + \frac{m}{4}\sin(\omega_2 T)\right] \end{Bmatrix} \tag{3}$$

$$E_{3+}(T) = \frac{\sqrt{2}}{4}E_2(T)\cdot\begin{Bmatrix} -\sin\left[\frac{m}{4}\sin(\omega_1 T) + \frac{m}{4}\sin(\omega_2 T)\right] \\ -j\cos\left[\frac{m}{4}\sin(\omega_1 T) + \frac{m}{4}\sin(\omega_2 T)\right] \\ +\cos\left[\frac{m}{4}\cos(\omega_1 T) + \frac{m}{4}\cos(\omega_2 T)\right] \\ -j\sin\left[\frac{m}{4}\cos(\omega_1 T) + \frac{m}{4}\cos(\omega_2 T)\right] \end{Bmatrix} \tag{4}$$

where $m = \pi V_0/V_\pi$ is the modulation index, and V_π is the half-wave voltage. After counter-propagating through DCF2, the frequency-domain optical fields injected into two PDs can be calculated as

$$E_{4\pm}(\omega) = E_{3\pm}(\omega)\exp\left(\frac{j}{2}\beta_2 L_2\omega^2\right) \tag{5}$$

where L_2 is the length of DCF2. Finally, the output currents of two PDs can be expressed as

$$I_\pm(T) = \frac{1}{2}nc\varepsilon_0 A_{eff} R_{PD} E_{4\pm}(T)\, E_{4\pm}^*(T) \tag{6}$$

where $E_{4\pm}(T)$ is the time-domain optical fields injected into two PDs. R_{PD} is the detector responsivity. c and ε_0 are the light velocity and the permittivity in vacuum, respectively. n and A_{eff} are the refractive index and the effective mode area of the fiber, respectively.

Supposing the optical bandwidth is much larger than the electrical one, the output currents of two PDs can be written as

$$I_{\pm}(T) = I_{\text{env}}(T) \cdot \left\{ \begin{array}{l} 2{J_0}^4\left(\frac{m}{4}\right) \\ \pm 4\sqrt{2}{J_0}^3\left(\frac{m}{4}\right) J_1\left(\frac{m}{4}\right) \cos\left(\frac{\omega_1}{M}T - {\omega_1}^2\varphi_{\text{dip}} + \frac{\pi}{4}\right) \\ \pm 4\sqrt{2}{J_0}^3\left(\frac{m}{4}\right) J_1\left(\frac{m}{4}\right) \cos\left(\frac{\omega_2}{M}T - {\omega_2}^2\varphi_{\text{dip}} + \frac{\pi}{4}\right) \\ +8{J_0}^3\left(\frac{m}{4}\right) J_2\left(\frac{m}{4}\right) \cos\left(\frac{2\omega_1}{M}T\right) \sin\left[(2\omega_1)^2\varphi_{\text{dip}}\right] \\ +8{J_0}^3\left(\frac{m}{4}\right) J_2\left(\frac{m}{4}\right) \cos\left(\frac{2\omega_2}{M}T\right) \sin\left[(2\omega_2)^2\varphi_{\text{dip}}\right] \\ -8{J_0}^2\left(\frac{m}{4}\right) {J_1}^2\left(\frac{m}{4}\right) \cos\left(\frac{\omega_2-\omega_1}{M}T\right) \cos\left[(\omega_2-\omega_1)^2\varphi_{\text{dip}}\right] \\ +8{J_0}^2\left(\frac{m}{4}\right) {J_1}^2\left(\frac{m}{4}\right) \cos\left(\frac{\omega_2+\omega_1}{M}T\right) \sin\left[(\omega_2+\omega_1)^2\varphi_{\text{dip}}\right] \\ +8{J_0}^2\left(\frac{m}{4}\right) {J_1}^2\left(\frac{m}{4}\right) \cos\left(\frac{\omega_2-\omega_1}{M}T - {\omega_2}^2\varphi_{\text{dip}} + {\omega_1}^2\varphi_{\text{dip}}\right) \\ \pm 4\sqrt{2}{J_0}^2\left(\frac{m}{4}\right) J_1\left(\frac{m}{4}\right) J_2\left(\frac{m}{4}\right) \cos\left[\frac{3\omega_1}{M}T - {\omega_1}^2\varphi_{\text{dip}} + (2\omega_1)^2\varphi_{\text{dip}} - \frac{\pi}{4}\right] \\ \pm 4\sqrt{2}{J_0}^2\left(\frac{m}{4}\right) J_1\left(\frac{m}{4}\right) J_2\left(\frac{m}{4}\right) \cos\left[\frac{3\omega_2}{M}T - {\omega_2}^2\varphi_{\text{dip}} + (2\omega_2)^2\varphi_{\text{dip}} - \frac{\pi}{4}\right] \\ \pm 4\sqrt{2}{J_0}^2\left(\frac{m}{4}\right) J_1\left(\frac{m}{4}\right) J_2\left(\frac{m}{4}\right) \cos\left[\frac{2\omega_2-\omega_1}{M}T + {\omega_1}^2\varphi_{\text{dip}} - (2\omega_2)^2\varphi_{\text{dip}} + \frac{\pi}{4}\right] \\ \pm 4\sqrt{2}{J_0}^2\left(\frac{m}{4}\right) J_1\left(\frac{m}{4}\right) J_2\left(\frac{m}{4}\right) \cos\left[\frac{2\omega_1-\omega_2}{M}T + {\omega_2}^2\varphi_{\text{dip}} - (2\omega_1)^2\varphi_{\text{dip}} + \frac{\pi}{4}\right] \\ \mp 4\sqrt{2}{J_0}\left(\frac{m}{4}\right) {J_1}^3\left(\frac{m}{4}\right) \cos\left[\frac{2\omega_2-\omega_1}{M}T - {\omega_2}^2\varphi_{\text{dip}} + (\omega_2-\omega_1)^2\varphi_{\text{dip}} + \frac{\pi}{4}\right] \\ \mp 4\sqrt{2}{J_0}\left(\frac{m}{4}\right) {J_1}^3\left(\frac{m}{4}\right) \cos\left[\frac{2\omega_1-\omega_2}{M}T - {\omega_1}^2\varphi_{\text{dip}} + (\omega_2-\omega_1)^2\varphi_{\text{dip}} + \frac{\pi}{4}\right] \\ \mp 4\sqrt{2}{J_0}^2\left(\frac{m}{4}\right) J_1\left(\frac{m}{4}\right) J_2\left(\frac{m}{4}\right) \cos\left[\frac{2\omega_2-\omega_1}{M}T - (\omega_1-2\omega_2)^2\varphi_{\text{dip}} + \frac{\pi}{4}\right] \\ \mp 4\sqrt{2}{J_0}^2\left(\frac{m}{4}\right) J_1\left(\frac{m}{4}\right) J_2\left(\frac{m}{4}\right) \cos\left[\frac{2\omega_1-\omega_2}{M}T - (\omega_2-2\omega_1)^2\varphi_{\text{dip}} + \frac{\pi}{4}\right] \end{array} \right\} \quad (7)$$

where $M = (L_1 + L_2)/L_1$ is the stretch factor. $\varphi_{\text{dip}} = \beta_2 L_2/(2M)$ is the phase-shift factor caused by GVD. $J_n(x)$ is the Bessel function of the first kind. $I_{\text{env}}(T)$ is the envelope function described by

$$I_{env}(T) = \frac{1}{4} nc\varepsilon_0 A_{\text{eff}} R_{\text{PD}} E_0^2 \cdot \frac{1}{\sqrt{1 + \left(\frac{\beta_2(L_1+L_2)}{T_0^2}\right)^2}} \exp\left\{ -\frac{T^2}{T_0^2\left[1 + \left(\frac{\beta_2(L_1+L_2)}{T_0^2}\right)^2\right]} \right\}. \quad (8)$$

Clearly, it can be concluded from (7) that, first, the power penalties of the fundamental signals in the two photocurrents are removed thanks to the SSB modulation. However, extra frequency-related phase shifts are added to the signals, which introduce distortion in the time domain, especially for a signal with a large bandwidth. Fortunately, these phase shifts will not degrade the SNR even if the input signal frequency is located near the transmission null point of the DSB modulation scheme, and it can be compensated in the digital domain using the proposed phase compensation algorithm described below. Second, the fundamental components and the odd-order distortion ones in the expression of I_+ and I_- have an identical amplitude but an opposite sign, while the even-order spurs are completely equal. Thus, all the even-order distortion spurs can be eliminated through calculating the difference of I_+ and I_- in the digital domain. Thirdly, the pulse-envelope-induced distortion can be removed through dividing the difference of the two photocurrents by the sum of them. Therefore, a large SNR and broadband characteristic can be guaranteed by the SSB modulation and the phase-shift compensation algorithm, while the system linearity can be improved by adopting the complementary parallel architecture and the corresponding linearization processing.

Based on the above theoretical analysis, three critical signal processing steps are essential to realize the aforementioned favorable features. The first one is the differential operation, which is implemented through dividing the difference of the two photocurrents by the sum of them in the digital domain. Although the even-order distortions still exist in the denominator, the Taylor series

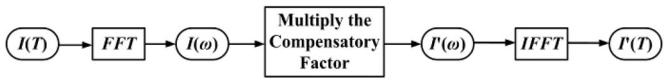

Fig. 2. Flow chart of the phase compensation algorithm. FFT: fast Fourier transform; IFFT: inverse fast Fourier transform.

expansion of the whole differential expression only reserves the product terms between the even-order components and the odd-order ones, indicating that the even-order distortions are completely removed while some weak odd-order components are generated. The second step is the arcsine operation, which is implemented through calculating the arcsine value of the output in the first step. The arcsine operation is theoretically effective to eliminate the odd-order distortions in a dispersion-free system employing a MZM, and has been demonstrated to suppress the odd-order spurs in a dual-output time-stretch system [15]. These two signal processing steps can be mathematically described by

$$I\,(T) = \arcsin\left[\frac{I_+(T) - I_-(T)}{I_+(T) + I_-(T)}\right]. \tag{9}$$

The third step is employing a phase-shift compensation algorithm to correct the dispersion-induced frequency-dependent phase shift in the signal term. The flow chart of the phase-shift compensation algorithm is presented in Fig. 2. First, the output data after the differential and arcsine operation is converted into the frequency domain using fast Fourier transform (FFT). Then, a pair of symmetric factors is multiplied on positive and negative frequency components in the frequency domain, respectively, to compensate the dispersion-induced frequency-dependent phase shift. Finally, inverse fast Fourier transform (IFFT) is implemented to convert the signal back into the time domain. After that, the dispersion-induced phase-shift-related time-domain distortion is rectified. The detail of the phase compensation principle is mathematically described as below.

The time-domain current after the differential and arcsine operation can be expressed as

$$I\,(T) = Q_1 \cos\left(\frac{\omega_1}{M}T - {\omega_1}^2\varphi_{\text{dip}} + \frac{\pi}{4}\right) + Q_2 \cos\left(\frac{\omega_2}{M}T - {\omega_2}^2\varphi_{\text{dip}} + \frac{\pi}{4}\right) + \cdots \tag{10}$$

where Q_1 and Q_2 are the coefficients of the two fundamental signals with different frequencies, respectively. After FFT, the expression of the current in the frequency domain is obtained as

$$\begin{aligned} I\,(\omega) = {} & \frac{1}{2}Q_1\delta\left(\omega - \frac{\omega_1}{M}\right)\exp\left(-i{\omega_1}^2\varphi_{\text{dip}} + i\frac{\pi}{4}\right) \\ & + \frac{1}{2}Q_1\delta\left(\omega + \frac{\omega_1}{M}\right)\exp\left(i{\omega_1}^2\varphi_{\text{dip}} - i\frac{\pi}{4}\right) \\ & + \frac{1}{2}Q_2\delta\left(\omega - \frac{\omega_2}{M}\right)\exp\left(-i{\omega_2}^2\varphi_{\text{dip}} + i\frac{\pi}{4}\right) \\ & + \frac{1}{2}Q_2\delta\left(\omega + \frac{\omega_2}{M}\right)\exp\left(i{\omega_2}^2\varphi_{\text{dip}} - i\frac{\pi}{4}\right) + \cdots \end{aligned} \tag{11}$$

where $\delta(x)$ is the unit impulse response function. In the frequency domain, a frequency-dependent phase factor of $\exp(i{\omega_n}^2\varphi_{\text{dip}} - i\pi/4)$ is multiplied on the positive frequency components, and a frequency-dependent phase factor of $\exp(-i{\omega_n}^2\varphi_{\text{dip}} + i\pi/4)$ is multiplied on the negative frequency components, where ω_n represents the corresponding angular frequency for each frequency component. For example, $\exp(i{\omega_1}^2\varphi_{\text{dip}} - i\pi/4)$ and $\exp(-i{\omega_1}^2\varphi_{\text{dip}} + i\pi/4)$ are the corresponding phase factors for the frequency components of ω_1 and $-\omega_1$, respectively, and $\exp(i{\omega_2}^2\varphi_{\text{dip}} - i\pi/4)$ and $\exp(-i{\omega_2}^2\varphi_{\text{dip}} + i\pi/4)$ are the corresponding phase factors for the frequency components of ω_2 and $-\omega_2$, respectively. After this phase compensation, the output frequency-domain current becomes

$$I'\,(\omega) = \frac{1}{2}Q_1\delta\left(\omega - \frac{\omega_1}{M}\right) + \frac{1}{2}Q_1\delta\left(\omega + \frac{\omega_1}{M}\right) + \frac{1}{2}Q_2\delta\left(\omega - \frac{\omega_2}{M}\right) + \frac{1}{2}Q_2\delta\left(\omega + \frac{\omega_2}{M}\right) + \cdots \tag{12}$$

TABLE 1
Parameters of the Optical Source and DCFS

Physical Quantity	Values and Units
central wavelength of the optical pulse	1555 nm
full width at half maximum of the optical pulse	210 fs
peak power of the optical pulse	973 W
GVD coefficient of the DCF	−130 ps/km/nm
length of the DCF1	1.3 km
length of the DCF2	11.7 km

whose IFFT is

$$I'(T) = Q_1 \cos\left(\frac{\omega_1}{M}T\right) + Q_2 \cos\left(\frac{\omega_2}{M}T\right) + \cdots \tag{13}$$

It can be seen from (13) that the GVD-induced frequency-dependent phase shift has been compensated and the phase-shift-induced distortion in the time domain has been corrected.

3. Simulation and Discussion

In this section, numerical simulation is implemented to verify the effectiveness of the proposed scheme, where the results are compared with those employing either a single dual-drive MZM via SSB modulation or a dual-output push-pull MZM via double-sideband (DSB) modulation. In the single dual-drive MZM scheme, the carrier envelope is artificially removed through a simple division operation [21]. In the dual-output push-pull MZM scheme, the differential operation and arcsine one are used to remove the carrier envelope and suppress the harmonic distortion [15]. Ultra-short optical pulses with a hyperbolic secant shape are used in the simulation as the optical carrier, which agrees with the situation adopting a passive mode-locked laser as the optical source [22]. Two RF signals with equal amplitude and different frequency of 12 GHz and 21 GHz are combined to drive the MZMs, where the modulation index is set as 0.6. An electronic ADC with a quantization level of 12 bits and a sampling rate of 10 GSa/s is applied to carry out the digitization process. The parameters of the optical source and the DCFs are shown in Table 1, which corresponds to a 10-fold stretch factor. The generalized nonlinear Schrödinger equation (GNLSE) is numerically solved to simulate the optical pulse propagation through the DCFs [23].

Fig. 3 exhibits the output spectra of the three schemes, in which the ratios of the signal to the harmonics are marked. Clearly, the pulse envelope has been removed, and the RF frequencies are down-converted from 12 GHz and 21 GHz to 1.2 GHz and 2.1 GHz through a 10-fold time stretch. Most importantly, it can be summarized from Fig. 3 as follows. First, the even-order distortions are large in the output spectrum of the single dual-drive MZM scheme as shown in Fig. 3(a), which stringently restrains the linearity of the time stretch process. As a contrast, they are canceled by employing the differential operation in the dual-output push-pull MZM scheme as shown in Fig. 3(b) and in the proposed parallel complementary MZM scheme as shown in Fig. 3(c), greatly improving the linearity performance. Second, the signal at frequency of 2.1GHz deteriorates by 16.6 dB in Fig. 3(b) due to the dispersion-induced power penalty effect in the DSB modulation scheme. On the contrary, the power penalty is completely removed in Fig. 3(a) and (c) thanks to the SSB modulation, which breaks the time-bandwidth limitation. Fig. 4 shows the transmission characteristic of a single-shot photonic time-stretch digitizer which employs the dual-output push-pull MZM via DSB modulation (dash dot line) and the proposed one via SSB modulation (solid line). Third, the

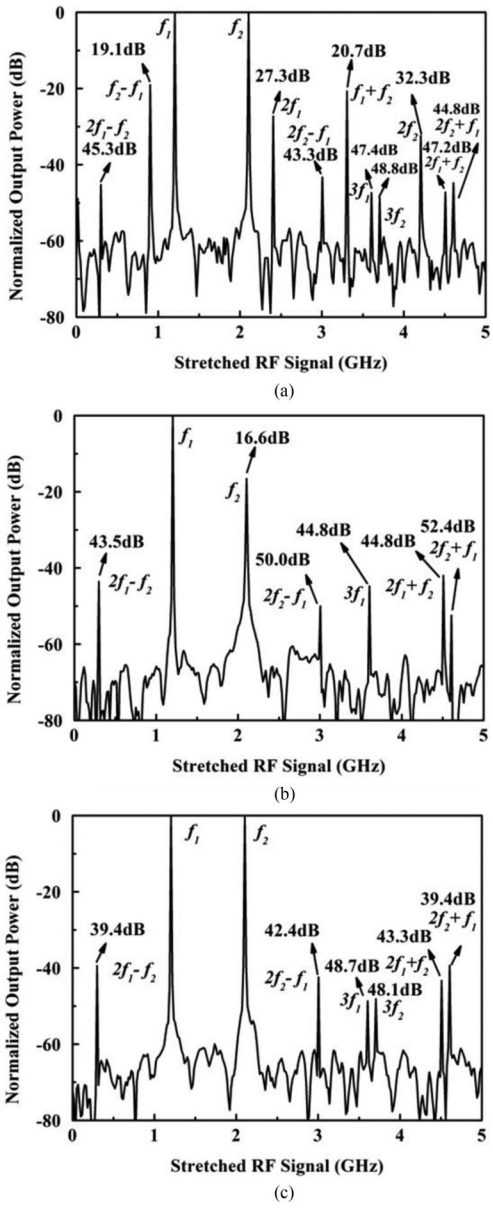

Fig. 3. Output spectra employing (a) a single dual-drive MZM via SSB modulation, (b) a dual-output push-pull MZM via DSB modulation, and (c) the proposed scheme.

noise floor in Fig. 3(b), (c) is lower than that in Fig. 3(a) since the differential operation can help enhance the SNR. Therefore, the proposed parallel complementary SSB modulation scheme with the assist of differential operation is efficient to simultaneously remove the pulse-envelope-induced distortion, the dispersion-induced power penalty and the even-order distortion products, and it can also improves the SNR. It should be noted that the spur with frequencies of $2f_2+f_1$ and $3f_2$, as presented in Fig. 3, are the aliased versions produced by the band-pass sampling (or namely down-conversion sampling). In the real application, those spurs with high frequencies will be filtered out due to the limited analog bandwidth of the electronic ADC. However, they are all reserved in the simulation by assuming that the bandwidth of the electronic ADC is sufficient, in order to highlight the effectiveness of the distortion suppression in the digital domain.

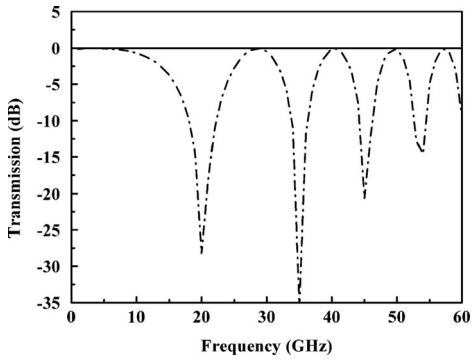

Fig. 4. Transmission characteristic of a single-shot photonic time-stretch digitizer employing the dual-output push-pull MZM via DSB modulation (dash dot line) and the proposed scheme via SSB modulation (solid line).

Additionally, it can also be found in Fig. 3 that the arcsine operation does not work in suppressing the odd-order distortions. For example, compared with those in Fig. 3(a), the component with the frequency of $3f_1$ in Fig. 3(c) is suppressed by 1.3 dB, while the components with the frequencies of $2f_1 - f_2$, $2f_2 - f_1$, $3f_2$, $2f_1 + f_2$ and $2f_2 + f_1$ are increased by 5.9 dB, 0.9 dB, 0.7 dB, 3.9 dB and 5.14 dB, respectively. This disability of arcsine operation can be explained as follows. The arcsine operation is capable of eliminating the odd-order distortions only in a dispersion-free case [15]. In a dispersive system, its effectiveness relies on the dispersion value which depends on the frequency of the RF signals and the length of the DCFs. Nevertheless, in-depth theoretical and simulation research indicates that the arcsine operation will not dramatically deteriorate the linearity even in the worst case, and it can bring a great benefit in suppressing the odd-order distortions for many frequencies. Fig. 5 manifests the effectiveness of the arcsine operation, where the two input RF signals are with frequencies of 3 GHz and 4 GHz, respectively. Fig. 5(a) exhibits the output spectrum of the scheme employing a single dual-drive MZM via SSB modulation, while Fig. 5(b) and (c) show the output spectra of the proposed scheme with and without arcsine operation, respectively. Clearly, compared with those in Fig. 5(a), the odd-order components with frequencies of $2f_1 - f_2$, $2f_2 - f_1$, $3f_1$, $2f_1 + f_2$, $2f_2 + f_1$ and $3f_2$ in Fig. 5(c) are suppressed by 18.4 dB, 13.2 dB, 5.8 dB, 12.7 dB, 7.6 dB and 7.7 dB, respectively. Besides, all the odd-order distortion components in Fig. 5(c) are lower than those in Fig. 5(b). In summary, arcsine operation does not always suppress the odd-order components, which is influenced by the frequency of the RF signals for a certain dispersive system. However, the operation is extremely effective for some RF frequencies, and it does not dramatically deteriorate the linearization performance even in its worst case. Therefore, the arcsine operation can still be taken into account to suppress the odd-order distortion in the practical application where the dispersion always exists.

Fig. 6(a)–(d) present the input RF signal, the output signal of the digitizer employing the dual-output push-pull MZM via DSB modulation, the output signal of the digitizer employing the proposed scheme without phase compensation and with it in the time domain, respectively. Apparently, the output signal in Fig. 6(b) is seriously distorted due to the frequency-dependent attenuation as shown in Fig. 3(b). Although the SSB modulation can eliminate this frequency-dependent power penalty, the output signal without phase compensation is still distorted in the time domain as shown in Fig. 6(c). Fortunately, this frequency-dependent phase-shift-induced time-domain distortion can be efficiently corrected using the proposed phase compensation algorithm, as shown in Fig. 6(d).

4. Analysis of Deviation

In the SSB modulation architecture utilizing a dual-drive MZM and a RF hybrid coupler, the vestigial sideband is inevitably produced by the asymmetry of the RF hybrid coupler and the modulator electrode, which may lead to residual power penalty, degrading the SNR and even putting a limit

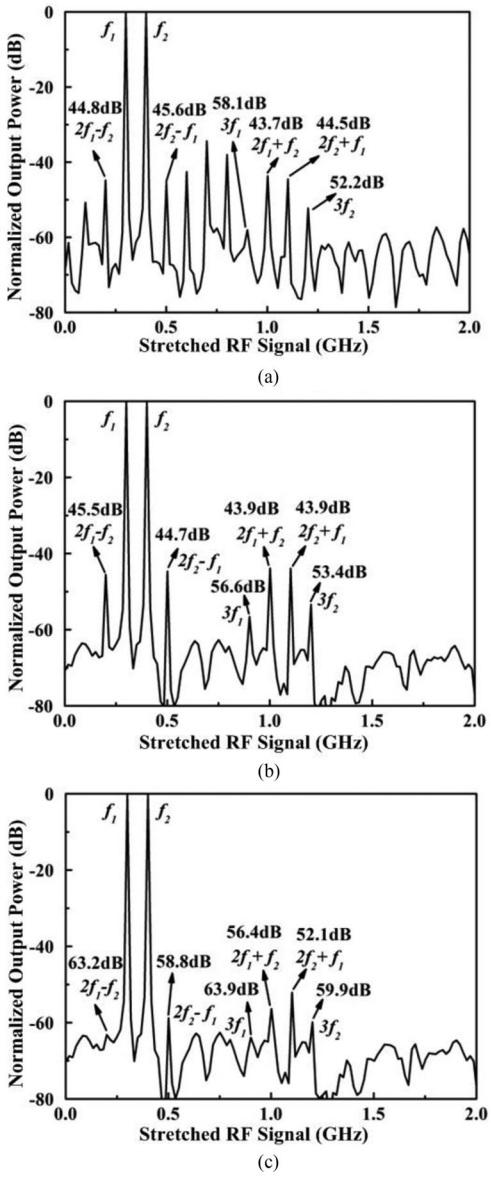

Fig. 5. Output spectra of (a) the scheme employing a single dual-drive MZM via SSB modulation, (b) the proposed scheme with differential operation but without arcsine operation, and (c) the proposed scheme with both differential and arcsine operation.

on the bandwidth [24]. In the proposed parallel SSB modulation scheme, the output optical fields of the two MZMs can be written as

$$E_{3-}(T) = \frac{\sqrt{2}}{4} E_2(T) \left\{ \begin{array}{l} \exp\left(j\left[\frac{\pi}{2} + \frac{m}{4}\cos(\omega_1 T)\right]\right) \\ +\exp\left(j\frac{m\gamma_1}{4}\sin(\omega_1 T + \Delta\phi_1)\right) \end{array} \right\} \tag{14}$$

$$E_{3+}(T) = \frac{\sqrt{2}}{4} E_2(T) \left\{ \begin{array}{l} \exp\left(j\left[\frac{3\pi}{2} - \frac{m\gamma_2}{4}\sin(\omega_1 T + \Delta\phi_2)\right]\right) \\ +\exp\left(-j\frac{m}{4}\cos(\omega_1 T)\right) \end{array} \right\} \tag{15}$$

where γ_1 and $\Delta\phi_1$ are the amplitude-imbalance ratio and the phase offset between the 90-degree-phase-shift RF port and the phase-shift-free RF port of the first dual-drive MZMs, respectively (ideal condition: $\gamma_1 = 1$, $\Delta\phi_1 = 0$). γ_2 and $\Delta\phi_2$ are the amplitude-imbalance ratio and the phase

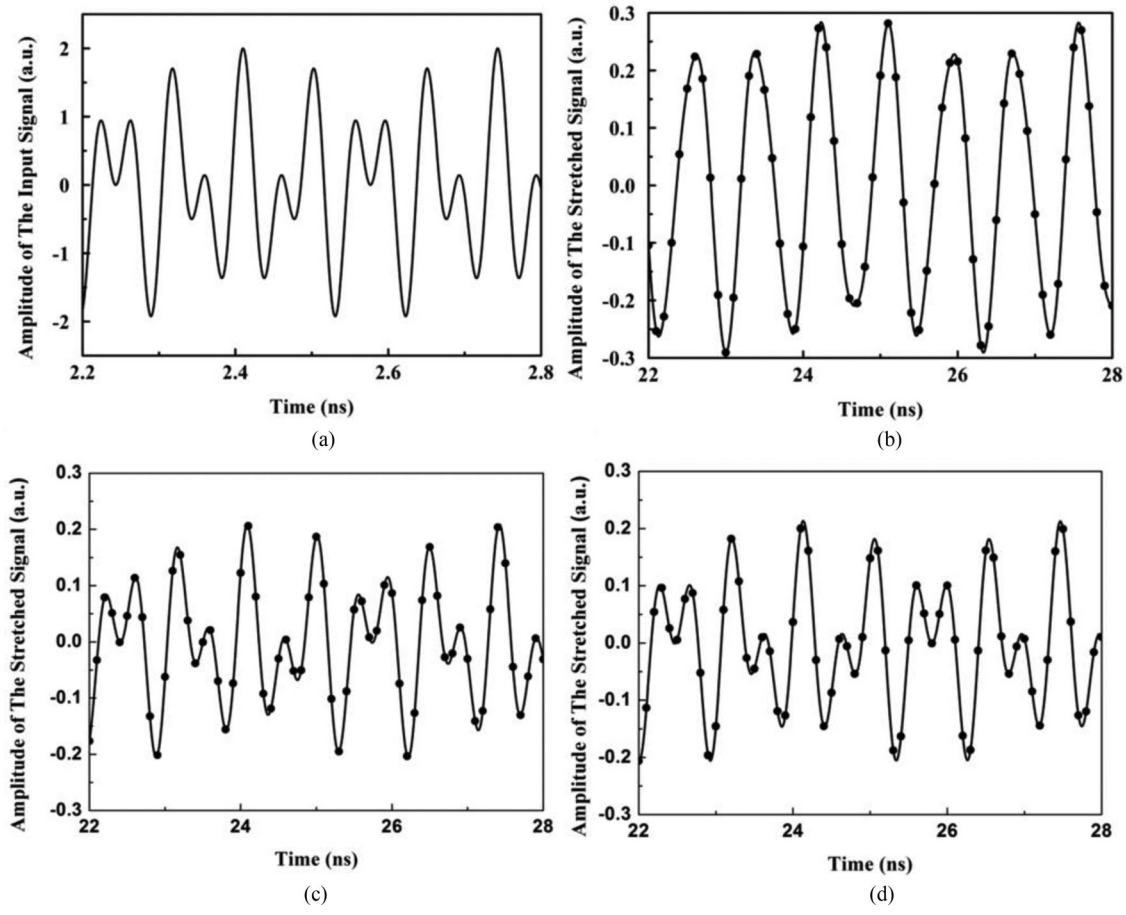

Fig. 6. (a) Input RF signal, (b) output signal of the digitizer employing the dual-output push-pull MZM via DSB modulation, (c) output signal of the digitizer employing the proposed scheme without phase compensation, and (d) output signal of the digitizer employing the proposed scheme with phase compensation.

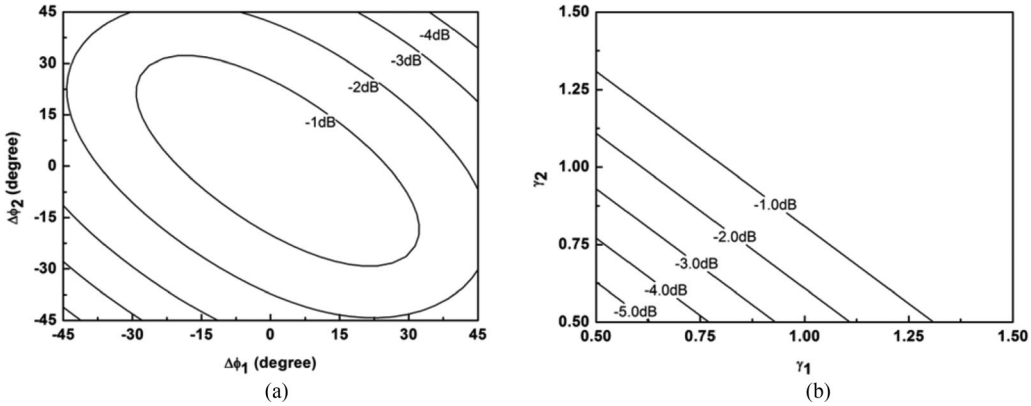

Fig. 7. Maximum power penalty in the proposed scheme under (a) various phase offsets of $\Delta\phi_1$ and $\Delta\phi_2$ without amplitude imbalances and (b) various amplitude-imbalance ratios of γ_1 and γ_2 without phase offsets.

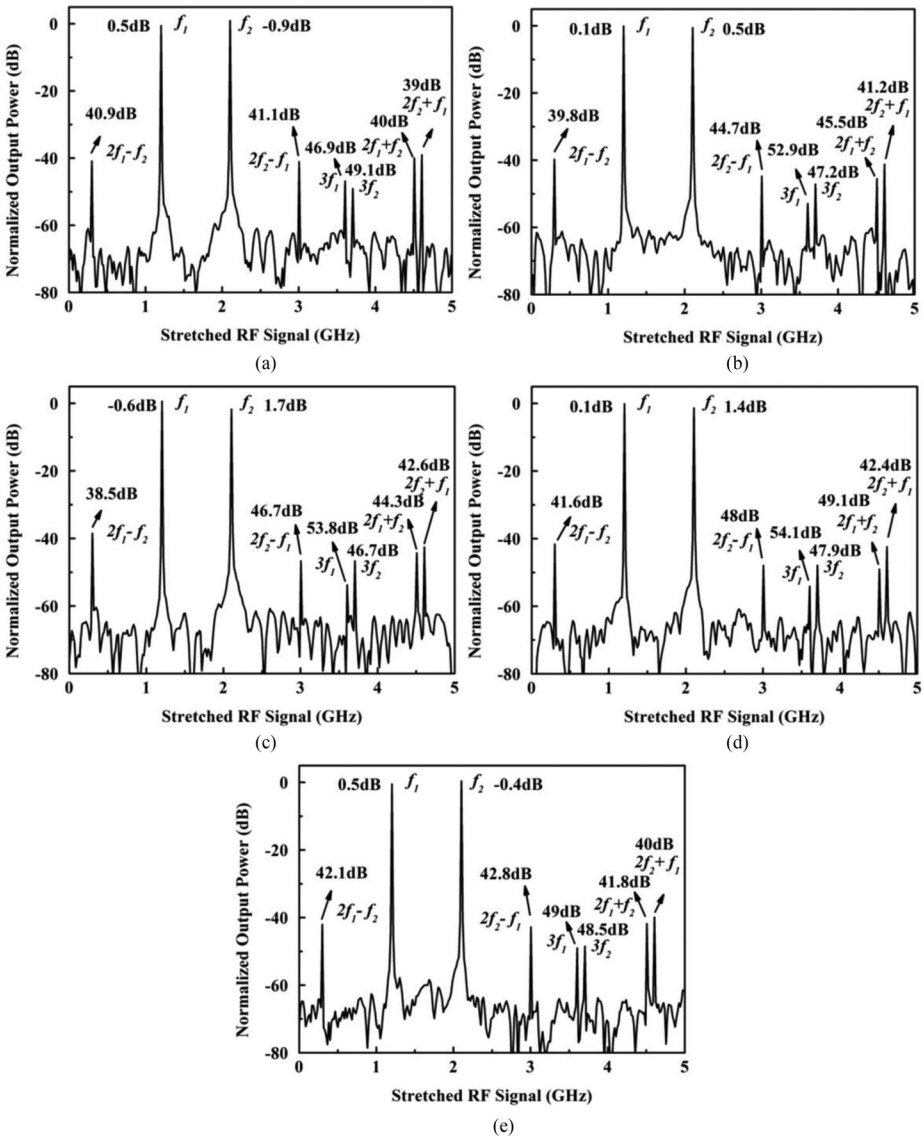

Fig. 8. Output spectra of the proposed scheme with (a) phase offsets of 14°, (b) amplitude-imbalance ratios of 0.9, (c) phase offsets of −20°, (d) amplitude-imbalance ratios of 0.75, and (e) phase offsets of 14° and amplitude-imbalance ratios of 0.9.

offset between the 90-degree-phase-shift RF port and the phase-shift-free RF port of the second dual-drive MZMs, respectively (ideal condition: $\gamma_2 = 1$, $\Delta\phi_2 = 0$). Ignoring the distortion spurs, the output current after the differential operation become

$$\frac{I_+(T) - I_-(T)}{I_+(T) + I_-(T)} \approx \frac{\sqrt{2}}{4} m \cos\left(\frac{\omega_1}{M} T\right) \sin\left({\omega_1}^2 \varphi_{dip} + \frac{\pi}{4}\right) - \frac{\sqrt{2}}{8} m \cos\left({\omega_1}^2 \varphi_{dip} + \frac{\pi}{4}\right) \cdot \left[\gamma_1 \sin\left(\frac{\omega_1 T}{M} + \Delta\phi_1\right) + \gamma_2 \sin\left(\frac{\omega_1 T}{M} + \Delta\phi_2\right)\right]. \quad (16)$$

It can be concluded from (16) that the power penalty can be eliminated only when the two MZMs are both driven by orthogonal RF signals with equal amplitude (i.e., $\gamma_1 = \gamma_2 = 1$, $\Delta\phi_1 = \Delta\phi_2 = 0$). Any deviation of γ_1, γ_2, $\Delta\phi_1$ and $\Delta\phi_2$ may lead to frequency-dependent power fluctuation.

Fig. 7 gives the contour map presenting the maximum power penalty according to (16). Specifically, Fig. 7(a) shows the maximum power penalty under various phase offsets of $\Delta\phi_1$ and $\Delta\phi_2$, where the amplitude imbalances are absent (i.e., $\gamma_1 = \gamma_2 = 1$). Fig. 7(b) displays the maximum power penalty under various amplitude imbalances of γ_1 and γ_2, where the phase offsets are ignorable (i.e., $\Delta\phi_1 = \Delta\phi_2 = 0$). The calculating results indicate that, instead of merely bringing residual power penalty in the single SSB modulation scheme [6], the vestigial sideband in the proposed parallel SSB modulation scheme leads to either a power penalty (e.g., $\gamma_1 + \gamma_2 < 2$) or a slight power gain (e.g., $\gamma_1 + \gamma_2 > 2$). For a commercially available RF hybrid coupler, the typical amplitude-imbalance ratio and phase offset are ± 0.6 dB and $\pm 7^\circ$ (e.g., Anaren 90° hybrid coupler, Model# 10 029-3), respectively, which corresponds to an acceptable power penalty around 1 dB according to Fig. 7.

In order to examine the influence of the vestigial sideband on the linearization performance of the proposed scheme, Fig. 8 exhibits the output spectra with various parameter deviations, in which all the components are normalized by the signal power without parameter deviation in Fig. 3(c) and the ratios are marked. Obviously, a small power gain occurs at the frequencies of f_1 in Fig. 8(c) and f_2 in Fig. 8(a) and (e). Additionally, it can be found from Fig. 8 that the cancellation of the even-order harmonics and the suppression of the odd-order spurs still work efficiently under either large amplitude-imbalance ratios or large phase offsets, indicating that the vestigial sideband will not degrade the linearization performance of the proposed scheme.

Besides the influence of the vestigial sideband, the imbalance of the parallel architecture may degrade the linearization performance of the system. The imbalance originates from the diversity of the power between the parallel paths, which is induced by the imbalanced splitting ratio of the optical coupler, the unequal insertion loss of the MZMs and OCs, and the inconsistent response of the PDs. Further research indicates that, although this parallel architecture imbalance has no impact on the suppression of the third-order harmonics, the removal of the pulse envelope and the dispersion-induced penalty, it indeed has an influence on eliminating the even-order harmonics. Fortunately, this kind of deviation can be compensated through adding RF amplifiers between PDs and ADCs or corrected through equalization in the digital domain.

5. Conclusion

In summary, a single-shot photonic time-stretch digitizer scheme with dispersion penalty-free and linearization performance is proposed, which is based on parallel SSB modulation architecture with each modulator biased at the quadrature point of the rising and falling edges of the transmission curve, respectively. Both theoretical analysis and simulation results demonstrate that the SSB modulation scheme with assistance of the proposed phase compensation algorithm can eliminate the dispersion-induced penalty and maintain the SNR. In addition, the pulse-envelope-induced distortion as well as the modulation-induced even-order distortions can be entirely removed by employing the complementary parallel architecture and the differential operation in the digital domain. For a certain dispersion system, arcsine operation can be considered as an effective method to suppress the odd-order distortion at some frequencies. Although the effective bandwidth of the proposed scheme is still restrained below multi-tens of GHz by the operation bandwidth of the commercially available RF hybrid couplers, a large time-bandwidth product can also be obtained since both a large time aperture and a large stretch factor are theoretically attainable thanks to the removal of the dispersion-induced penalty. It should also be pointed out that the maximum time-bandwidth product is limited by the repetition rate of the MLL, the bandwidth of optical source and the degrading signal-to-noise ratio during the stretch process, which should be carefully considered in the design procedure.

In actual system implementation, the balance between the parallel paths should be carefully considered, which includes both the hardware consideration and the digital processing one. For the

hardware consideration, the RF hybrid couplers, the dual-drive MZMs, the optical circulators, the PDs and the ADCs should have consistent response. In addition, the optical and electrical couplers should have balanced splitting ratio. For the digital processing consideration, residual amplitude imbalance and time difference between the parallel paths should be compensated before the linearization operation. Additionally, the static frequency response difference between the parallel paths should also be calibrated in advance. Moreover, the cost and the power consumption of the proposed scheme just increase a little since only an extra dual-drive MZM and several inexpensive passive devices are supplemented compared with the scheme employing a dual-output push-pull MZM. Therefore, the proposed scheme is a promising one to realize single-shot photonic time-stretch digitizer with a large time-bandwidth product and linearization performance.

References

[1] J. A. Wepman, "Analog-to-digital converters and their applications in radio receivers," *IEEE Commun. Mag.*, vol. 33, no. 5, pp. 39–45, May 1995.

[2] R. H. Walden, "Performance trends for analog to digital converters," *IEEE Commun. Mag.*, vol. 37, no. 2, pp. 96–101, Feb. 1999.

[3] R. H. Walden, "Analog-to-digital converter in the early twenty-first century," in *Wiley Encyclopedia of Computer Science and Engineering*. Hoboken, NJ, USA: Wiley, 2008.

[4] R. H. Walden, "Analog-to-digital converter survey and analysis," *IEEE J. Sel. Areas Commun.*, vol. 17, no. 4, pp. 539–550, Apr. 1999.

[5] A. S. Bhushan, F. Coppinger, and B. Jalali, "Time-stretched analogue-to-digital convertion," *Electron. Lett.*, vol. 34, no. 11, pp. 1081–1083, May 1998.

[6] Y. Han and B. Jalali, "Photonic time-stretched analog-to-digital converter: Fundamental concepts and practical considerations," *J. Lightw. Technol.*, vol. 21, no. 12, pp. 3085–3103, Dec. 2003.

[7] J. Chou, J. Conway, G. Sefler, G. Valley, and B. Jalali, "150 GS/s real-time oscilloscope using a photonic front end," in *Proc. Asia-Pacific Microw. Photon. Conf.*, 2008, pp. 35–38.

[8] J. Chou, J. A. Conway, G. A. Selfler, G. C. Valley, and B. Jalali, "Photonic bandwidth compression front end for digital oscilloscopes," *J. Lightw. Technol.*, vol. 27, no. 22, pp. 5073–5077, Nov. 2009.

[9] J. Chou, O. Boyraz, D. Solli, and B. Jalali, "Femtosecond real-time single-shot digitizer," *Appl. Phys. Lett.*, vol. 91, no. 16, pp. 161105–161105-3, Oct. 2007.

[10] J. H. Wong *et al.*, "Generation of flat supercontinuum for time-stretched analog-to-digital converters," in *Proc. IEEE Quantum Electron. Conf. Lasers Electro-Opt.*, 2011, pp. 256–258.

[11] J. Han, B. J. Seo, Y. Han, B. Jalali, and H. R. Fetterman, "Reduction of fiber chromatic dispersion effects in fiber-wireless and photonic time-stretching system using polymer modulators," *J. Lightw. Technol.*, vol. 21, no. 6, pp. 1504–1509, Feb. 2003.

[12] J. Chou, T. S. Rose, J. A. Conway, G. C. Valley, and B. Jalali, "Time-gated filter for sideband suppression," *Opt. Lett.*, vol. 34, no. 7, pp. 869–871, Apr. 2009.

[13] Y. Han, O. Boyraz, and B. Jalali, "Ultrawide-band photonic time-stretch A/D converter employing phase diversity," *IEEE Trans. Microw. Theory*, vol. 53, no. 4, pp. 1404–1408, Apr. 2005.

[14] A. M. Fard, S. Gupta, and B. Jalali, "Photonic time-stretch digitizer and its extension to real-time spectroscopy and imaging," *Laser Photon. Rev.*, vol. 7, no. 2, pp. 207–263, 2013.

[15] S. Gupta, G. C. Valley, and B. Jalali, "Distortion cancellation in time-stretch analog-to-digital converter," *J. Lightw. Technol.*, vol. 25, no. 12, pp. 3716–3721, Dec. 2007.

[16] B. Xu *et al.*, "Spurious-free dynamic range improvement in a photonic time-stretched analog-to-digital converter based on third-order predistortion," *Photon. Res.*, vol. 2, no. 5, pp. 97–101, Oct. 2014.

[17] D. Peng, Z. Zhang, Y. Ma, Y. Zhang, S. Zhang, and Y. Liu, "Broadband linearization in photonic time-stretch analog-to-digital converters employing an asymmetrical dual-parallel Mach-Zehnder modulator and a balanced detector," *Opt. Exp.*, vol. 24, no. 11, pp. 11546–11557, May 2016.

[18] J. Stigwall and S. Galt, "Signal reconstruction by phase retrieval and optical backpropagation in phase-diverse photonic time-stretch systems," *J. Lightw. Technol.*, vol. 25, no. 10, pp. 3017–3027, Oct. 2007.

[19] S. Gupta, B. Jalali, J. Stigwall, and S. Galt, "Demonstration of distortion suppression in photonic time-stretch ADC using back propagation method," in *Proc. IEEE Int. Top. Meeting Microw. Photon.*, 2007, pp. 141–144.

[20] A. Fard, S. Gupta, and B. Jalali, "Broadband linearization and its application to photonic time-stretch ADC," in *Proc. IEEE Int. Top. Meeting Microw. Photon.*, 2010, pp. 238–240.

[21] X. Xie, X. Yin, S. Li, L. Li, X. Xin, and C. Yu, "Photonic time-stretch analog-to-digital converter employing envelope removing technique," *Optik*, vol. 125, no. 9, pp. 2195–2198, Oct. 2014.

[22] L. E. Nelson, D. J. Jones, K. Tamura, H. A. Haus, and E. P. Ippen, "Ultrashort-pulse fiber ring lasers," *Appl. Phys. B.*, vol. 64, no. 2, pp. 277–294, Aug. 1997.

[23] G. P. Agrawal, *Nonlinear Fiber Optics*. New York, NY, USA: Academic, 2012.

[24] Y. Han and B. Jalali, "Time-bandwidth product of the photonic time-stretched analog-to-digital converter," *IEEE Trans. Microw. Theory*, vol. 51, no. 7, pp. 1886–1892, Jul. 2003.